*Annals of Glaciology* 34 2002


# Iceberg calving from the Amery Ice Shelf, East Antarctica

Helen A. Fricker,[1] Neal W. Young,[2] Ian Allison,[2] Richard Coleman[3,4]
[1]*Institute of Geophysics and Planetary Physics, Scripps Institution of Oceanography, University of California San Diego, La Jolla, CA 92093-0225, U.S.A.*
[2]*Antarctic CRC and Australian Antarctic Division, Hobart, Tasmania 7001, Australia*
[3]*Antarctic CRC and School of Geography and Environmental Studies, University of Tasmania, Box 252-80, Hobart, Tasmania 7001, Australia*
[4]*CSIRO Marine Research, Box 1538, Hobart, Tasmania 7001, Australia*

ABSTRACT. We investigate the iceberg-calving cycle of the Amery Ice Shelf (AIS), East Antarctica, using evidence acquired between 1936 and 2000. The most recent major iceberg-calving event occurred between late 1963 and early 1964, when a large berg totalling about 10 000 km$^2$ in area broke from the ice front. The rate of forward advance of the ice front is presently 1300–1400 m a$^{-1}$. At this rate of advance, based on the present ice-front position from recent RADARSAT imagery, it would take 20–25 years to attain the 1963 (pre-calve) position, suggesting that the AIS calving cycle has a period of approximately 60–70 years. Two longitudinal (parallel-to-flow) rifts, approximately 25 km apart at the AIS front, are observed in satellite imagery acquired over the last 14+ years. These rifts have formed at suture zones in the ice shelf, where neighbouring flow-bands have separated in association with transverse spreading. The rifts were 15 km (rift A) and 26 km (rift B) in length in September 2000, and will probably become the sides of a large tabular iceberg (25 km × 25 km). A transverse (perpendicular-to-flow) fracture, visible at the upstream end of rift A in 1996, had propagated 6 km towards rift B by September 2000; when it meets rift B the iceberg will calve. A satellite image acquired in 1962 shows an embayment of this size in the AIS front, hence we deduce that this calving pattern also occurred during the last calving cycle, and therefore that the calving behaviour of the AIS apparently follows a regular pattern.

## 1. INTRODUCTION

Most of the mass loss from the Antarctic ice sheet takes place in the ice shelves and glacier tongues, via iceberg calving from their fronts or basal melting from below (Jacobs and others, 1992). Large iceberg-calving events generate great interest amongst not only scientists but also the general public, because an increase in these types of events could be an indicator of climate change. Iceberg-calving events are episodic in nature and may produce icebergs with size ranging from a few hundred metres up to many tens of kilometres (Young and others, 1998). The time interval between events for any given part of the ice margin may range from one to a few years and up to many decades. In order to determine whether calving rates are changing, it is necessary to first establish the normal calving rate. Monitoring of iceberg-calving events from Antarctic ice shelves using satellite imagery has become commonplace (e.g. Ferrigno and Gould, 1987). The ice shelves of the West Antarctic ice sheet (WAIS) have been subjects of recent scrutiny since they have produced several giant icebergs over the last 2 years (Lazzara and others, 1999). Icebergs of significant size that calved from the East Antarctic ice sheet (EAIS) over the same time interval came from the Ninnis Glacier tongue in the 1999/2000 austral summer (personal communication from R. A. Massom, 2001), although these icebergs are smaller than their WAIS counterparts.

The Amery Ice Shelf (AIS) is the largest ice shelf in East Antarctica. It drains the grounded portion of the Lambert Glacier–Amery Ice Shelf system (Lambert–Amery system), which accounts for 1.6 × 10$^6$ km$^2$ of the grounded EAIS (16% of its total area). The mass flux from the interior of the system, measured along a traverse approximately following the 2500 m contour line, is 44 Gt a$^{-1}$ (Fricker and others, 2000b). This flux, plus additional ice that accumulates downstream of the traverse route, flows towards the coast in a convergent pattern that is focused through the front of the AIS, which accounts for only 2% (~200 km) of the East Antarctic coastline. In this paper, we investigate the AIS in terms of potential future calving, to assess the likelihood of large bergs calving from this ice shelf in the near future. We also discuss features, observed in recent RADARSAT synthetic aperture radar (SAR) imagery and a European Remote-sensing Satellite (ERS-1/-2) tandem-mission SAR interferogram, that are precursors to an iceberg calving event.

## 2. AIS ICEBERGS

### 2.1. Last major calving event

The last major calving event from the AIS was in late 1963 or early 1964, when a massive tabular iceberg about 10 000 km$^2$ in area calved (Budd, 1966). The berg split into two smaller bergs a year later, which were carried westwards from Prydz Bay in the East Wind Drift (EWD), close to the coast of Antarctica. In 1967 one of the bergs (denominated 1967B, with dimensions 110 km × 75 km) collided with the Trolltunga ice tongue in the Fimbul Ice Shelf at 1° W, and this collision initiated the calving of the Trolltunga iceberg

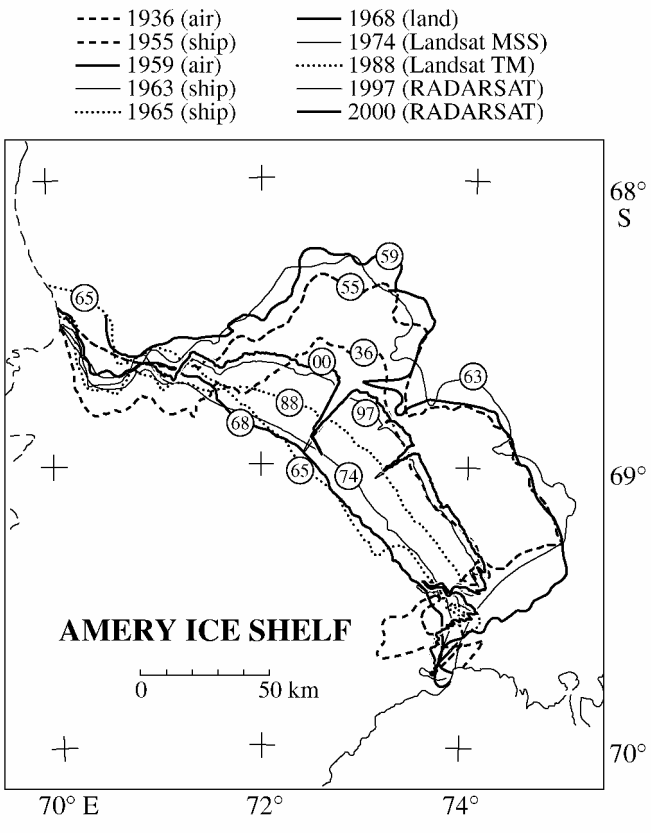


*Fig. 1. AIS front positions for 10 epochs between 1936 and 2000. These locations were obtained using different methods, as outlined in the legend. Animated version can be seen at http://rai.ucsd.edu/~helen/Annals2001/Fig1_ANIM.gif.*

(named 1967A), which was 104 km × 53 km in dimension (Swithinbank and others, 1977). This is an example of the collision theory of iceberg calving which was postulated by Swithinbank and others (1977). A recent example of this type of event occurred on the Ross Ice Shelf in September 2000, when iceberg B15-A (US National Ice Center nomenclature) dislodged C16 from the ice front. Attenuation of radio-echo sounding (RES) echoes observed over one of the Amery-derived icebergs in 1969 indicated that there was marine ice at the base of the berg (Swithinbank and others 1977; see section 2.2).

Between 1936 and 1968, the position of the AIS front was recorded by various survey methods: airborne, shipborne and terrestrial (Robertson, 1992). Since the early 1970s the front has also been captured in Landsat Multispectral Scanner (MSS) and Thematic Mapper (TM) imagery and, more recently, in RADARSAT SAR imagery. Figure 1 shows ice-front positions surveyed at six epochs between 1936 and 1968, in 1974 (Landsat MSS) and 1988 (Landsat TM) and in 1997 and 2000 in RADARSAT SAR imagery. The difference between the 1963 and 1965 fronts shows the approximate area of the iceberg that calved in 1963–64 (~140 km transverse by ~70 km longitudinal), approximately 14% of the current area of the AIS (69 000 km$^2$). The sequence after 1965 shows how the ice shelf propagates forward after the calving. As the front advances, it bulges outwards in the centre as a result of higher velocities there (see section 3.2). (The whole sequence from 1936 to 2000 can be viewed as an animation at: http://rai.ucsd.edu/~helen/Annals2001/Fig1_ANIM.gif.) Zwally and others (2002) estimate a mean annual rate of forward advance of the AIS front of 1.03 ± 0.04 km a$^{-1}$ for the period 1978–95 from satellite radar altimetry.

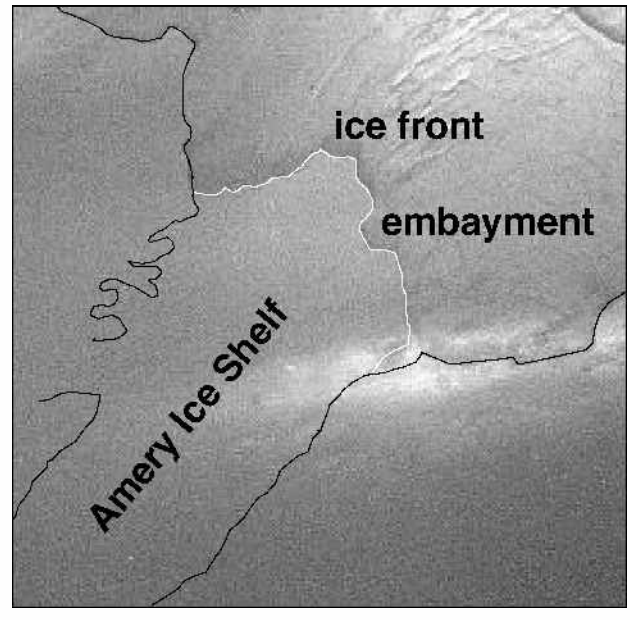


*Fig. 2. DISP image of the AIS front acquired in May 1962. The image is severely affected by cloud, but the ice front can be discerned.*

Recently declassified Defense Intelligence Satellite Program (DISP) satellite photographs show the AIS front in May 1962, about 18 months before the calving event. Although these images are severely affected by thick cloud cover, it is possible to discern the coastline of Mac. Robertson Land and the front of the AIS in the images (Fig. 2). At that time, the ice shelf protruded far into Prydz Bay, much further than its present-day extent. There is clearly an embayment in the ice front, suggesting that a smaller iceberg had calved from this location prior to the DISP photograph being taken. No icebergs are visible in Prydz Bay, so it is not possible to estimate when this smaller berg calved. However, there is also an embayment present in both the 1955 and 1959 locations (Fig. 1), indicating that the smaller calving event took place at least 8 years prior to the major calve. Differences in the shape of the embayment in these years possibly arise from errors associated with the survey methods used: shipborne survey using a sextant in 1955 and airborne survey via dead-reckoning in 1959. From the air, the presence or absence of fast ice inside the embayment could have led to interpretation errors.

### 2.2. Green icebergs

The AIS has been cited as a source of icebergs which have an emerald green appearance (Kipfstuhl and others, 1992), the colour being due to the presence of "marine" ice in the iceberg. Marine ice is deposited as a result of the "ice-pump" (Lewis and Perkin, 1986) mechanism that operates in the cavities beneath the ice shelves. The ice pump is driven by changes in melting and freeze rates associated with the dependence on pressure (depth) of the melting-point temperature. It results in melting near the (deep) grounding line and freezing onto the ice-shelf base at shallower depths further downstream, which redistributes ice under the ice shelf (Jacobs and others, 1992; Jenkins and Bombosch, 1995), forming a marine-ice layer beneath the ice shelf. Basal melt rates under the AIS are high near the grounding line, on the order of tens of metres per annum (Fricker and others, in press). The thickness of the marine-ice layer can be estimated using a buoy-

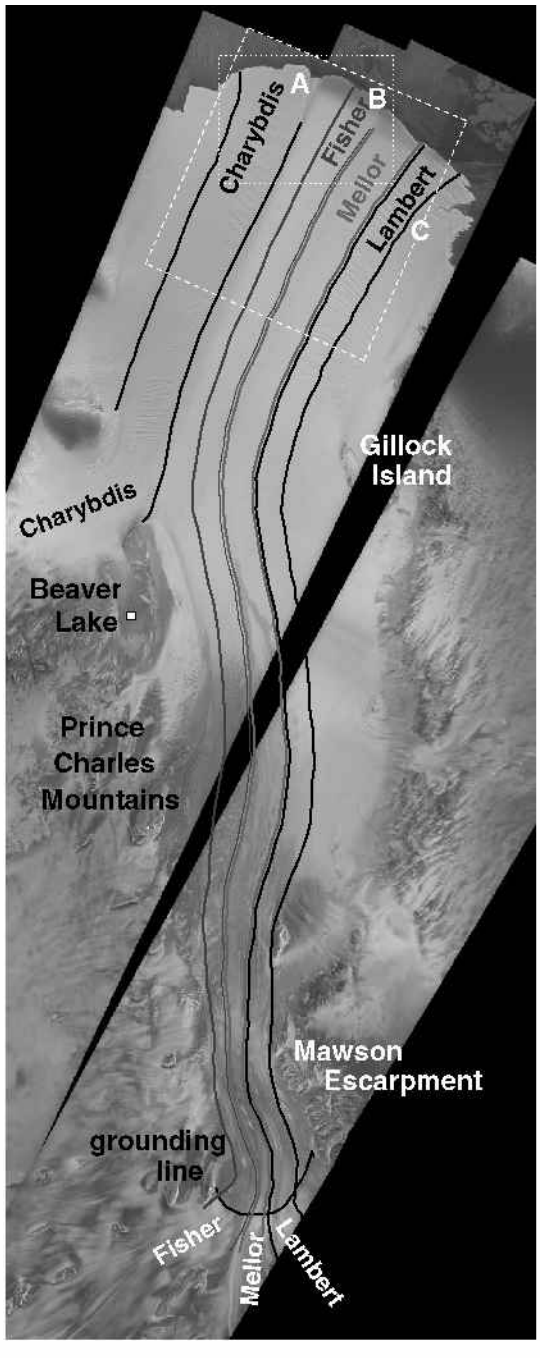


*Fig. 3. RADARSAT mosaic of the Lambert–Amery system compiled by I. Joughin. RADARSAT data were collected during MAMM and are copyright to the Canadian Space Agency. White dotted and dashed lines indicate the approximate extents of Figures 5 and 6, respectively.*

ancy relation if surface height and ice-thickness information from RES are available. This technique works because the RES signal does not penetrate the marine ice, so an anomaly exists in the difference between the theoretical ice thickness derived from the height data and the measured thickness. Fricker and others (2001) did this calculation for the AIS and found that the marine ice is confined to the northwestern quadrant, and is oriented along two longitudinal bands, each up to 190 m thick.

The pattern of marine ice underneath the AIS is significantly different to that beneath the Ross and Ronne Ice Shelves, and similar to that of the Filchner Ice Shelf (FIS; Grosfeld and others, 1998), in that it persists all the way to the calving front. Under the Ross and Ronne Ice Shelves, the marine-ice basal layer is melted off towards the ice front by a warm sub-shelf current (Warren and others, 1993); there is no such current under the AIS. Therefore, when icebergs calve from the western front of the AIS, they still contain marine ice. These icebergs break into smaller bergs, and subsequent melting makes these bergs unstable, causing them to capsize and reveal their marine ice above the ocean surface. The green appearance of the marine ice derives from the great abundance of organic phytoplankton blooms in Prydz Bay: organic particles become trapped in the marine ice (Warren and others, 1993). The ice itself preferentially absorbs visible solar radiation at red wavelengths (causing ice to appear blue), and the organic particles absorb radiation at blue wavelengths so that the colour of marine ice is shifted from blue to green. Icebergs from the AIS drift westwards in the EWD which surrounds Antarctica, and it has been claimed that they drift as far as the Weddell Sea (Swithinbank and others, 1977; Kipfstuhl and others, 1992). Green icebergs are often observed west of the AIS near Mawson station.

## 3. CURRENT STATUS OF AIS

### 3.1. RADARSAT Antarctic Mapping Missions

SAR data acquired during the first Antarctic Mapping Mission (AMM-1) of the Canadian Space Agency RADARSAT satellite (in September and October 1997) were used to compile a complete mosaic of the Antarctic continent (Jezek, 1999). The second mission, the Modified Antarctic Mapping Mission (MAMM), took place between September and November 2000. Figure 3 contains a mosaic of the Lambert–Amery system compiled from MAMM by I. Joughin at the Jet Propulsion Laboratory (JPL), Pasadena, CA, and indicates the approximate location of the system's newly defined grounding line (Fricker and others, in press). The main tributary glaciers that flow into the confluence region near the grounding line are (from east to west) Lambert, Mellor and Fisher Glaciers. Charybdis Glacier joins the western part of the ice shelf downstream of Beaver Lake. The boundaries of four of the seven major flow-bands have been overlaid on the mosaic, in a manner similar to that of Hambrey and Dowdeswell (1994).

At the front of the shelf, two large longitudinal-to-flow (north–south) rifts (26 and 15 km long) are present (we call these rift A and rift B, respectively). These rifts extend from the ice-shelf surface to its base, and are filled with ice mélange (Rignot and MacAyeal, 1988) consisting of sea ice, ice-shelf fragments and wind-blown snow. These features most likely developed over the 1980s, and a Landsat image from February 1988 shows that they were 16 km (rift A) and 11 km (rift B) long at that time. Tracing the flow-bands back upstream shows that the rifts originate at the boundaries of major flow-bands: the westernmost (rift A) between the Charybdis flow-band and the band containing ice that entered the AIS across its western margin having passed through the Prince Charles Mountains; the easternmost (rift B) between the Fisher and Mellor flow-bands.

This location of the longitudinal rifts at the AIS front suggests that this type of rift formation is related to flow-band history and source, and is a result of stress patterns active long before and far upstream, that are preserved downstream as far as the ice front. The mechanical properties of ice in the suture zone, which has in general been subject to more deformation, are different to those of ice in between sutures, and represent a plane of weakness within the ice shelf. The flow-bands from

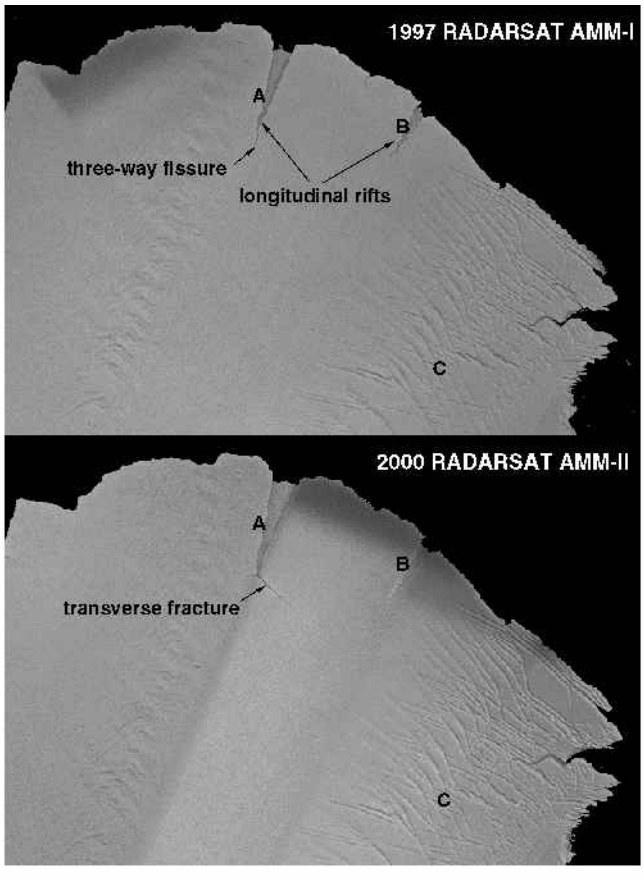


*Fig. 4. RADARSAT images over AIS front collected during AMM-1 (1997) and MAMM (2000). Animated version of this plot is online at http://rai.ucsd.edu/~helen/Annals2001/Fig4ANIM.gif.*

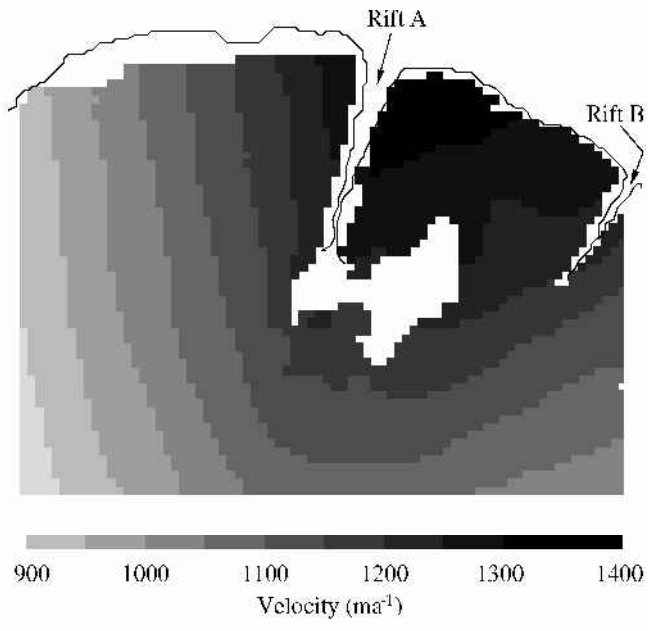


*Fig. 5. Magnitude of ice velocity over central part of AIS front, derived from maximum coherence tracking in a pair of SAR images acquired by RADARSAT on 28 September and 18 October 1997 (from Young and Hyland, 2002).*

the different inputs merge to form the AIS, which is confined for most of its length such that the ice flow is roughly parallel. However, when the AIS front protrudes past a critical limit into Prydz Bay, the high transverse strain rates in the ice cause the streams to separate from each other, forming longitudinal rifts. These rifts are precursors to iceberg-calving events: it appears that it is this "loose-tooth" section of ice shelf between these two rifts that calved away before the main calving event of 1963–64, leaving the embayment seen in Figure 2. The break-up of tabular icebergs can also occur along sutures, as occurred when B-15 split into B-15A and B-15B along the suture formed by Ice Stream D entering the Ross Ice Shelf (Lazzara and others, 1999). It is likely that when the giant iceberg that calved from the AIS in 1963–64 split a year after calving, it was along one of the suture zones causing the longitudinal rifts under discussion.

RADARSAT images from AMM-1 (1997) and MAMM (2000) over the AIS front are shown in Figure 4. In the top image, a three-way fissure is seen at the tip of rift A, and a short transverse-to-flow fracture (east–west) is seen. In the bottom image the three-way fissure has opened up in the 3 year interval between these images, and the transverse fracture is now well developed. The opening of the rift is seen more clearly in an animation of these images at: http://rai.ucsd.edu/~helen/Annals2001/Fig4ANIM.gif. The transverse fracture will probably become a future calving line, and the longitudinal rifts will form the iceberg sides once the transverse fracture meets rift B. This is different to calving on the Filchner–Ronne and Ross Ice Shelves, where the transverse fracture is typically present first and longitudinal rifts form later (Lazzara and others, 1999). The east–west (transverse-to-flow) rift associated with B-15 first appeared in the late 1980s, and grew to over 280 km length between 1992 and 1996. The B-15 calving event in March 2000 occurred when a short north–south (longitudinal-to-flow) rift, which was not visible in satellite imagery until after 1996, intersected the transverse rift (personal communication from D. R. MacAyeal, 2001). However, we do not believe that this is the pattern during large calving events of the AIS, such as that which occurred in 1963–64.

On the eastern side of the images, a third long rift (of a "zigzag" shape) is seen. The shape of this rift occurs as a result of the intersecting pattern of crevasses present on the east side of the shelf near the front (region C). These crevasses, around 40–50 km long, form downstream of Gillock Island, which disturbs the ice flow. These crevasses will ultimately lead to the formation of a transverse rift that will become the calving front for the next major calving event.

### 3.2. Ice-front velocities

Ice-front velocities have been derived for the AIS front from maximum coherence tracking in SAR imagery, using RADARSAT images from AMM-1 in September and October 1997 (Young and Hyland, 2002; Fig. 5). The RADARSAT-derived data show that the velocities over the loose tooth in the ice front are greater than in the surrounding region, and that the western part of the loose tooth moves around 80 m $a^{-1}$ faster than the ice immediately to the west of rift A. This is very much greater than the difference that exists purely as a result of the lateral velocity gradient across the front: velocities derived from feature tracking in 1988 Landsat imagery (prior to formation of the transverse fracture) show that the velocity difference across rift A was only 10 m $a^{-1}$. Between AMM-1 and MAMM the centre of the front advanced about 4 km (3 years), the velocity there presently being 1300–1400 m $a^{-1}$.

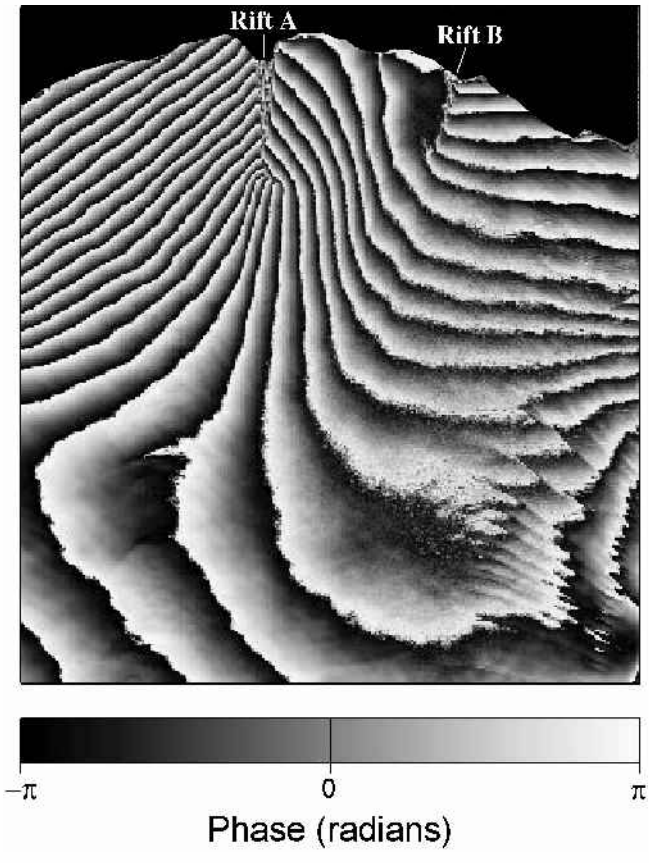


*Fig. 6. Interferogram derived from ERS-1 orbit 24526 (24 March 1996) and ERS-2 orbit 04309 (25 March 1996) of the eastern part of the AIS front. The topographic contribution to the phase has been removed using topography provided by a digital elevation model derived from ERS-1 satellite radar altimetry (Fricker and others, 2000a).*

### 3.3. SAR interferometry

We generated a SAR interferogram over the AIS front to examine the ice motion near the loose tooth. SAR interferometry (InSAR) is a well-established technique that has recently revolutionized our knowledge of many Antarctic ice-shelf and glacier systems (e.g. Rignot and others, 1997; Joughin and others, 1999). The theory on which InSAR is based has been discussed in detail elsewhere. Interferograms are formed between pairs of images that have been collected over the same area from almost the same satellite positions, but at different times. Over ice shelves, the phase change observed between the image pairs is composed of a relative topographic component (resulting from a parallax effect because the satellite location is not exactly the same for each pass) and a relative displacement component because each radar scatterer has moved in the intervening time between satellite passes (due to both tidal displacement and ice-shelf creep flow). The ERS-1 and -2 satellites operated in a "tandem mission", in which ERS-2 followed ERS-1 in its orbit, but 24 hours apart, between 21 March 1995 and 3 June 1996.

Figure 6 shows an interferogram generated from ERS-1 orbit 24526 and ERS-2 orbit 04853, repeats along a descending track which passed over the central AIS front on 24 and 25 March 1996, respectively. A phase change of $2\pi$ represents a relative displacement of 2.8 cm in the radar look direction (from right to left in this image). The relative topographic component of the phase change was removed using the synthesized phase signal from a digital elevation model for the ice shelf derived from ERS-1 satellite radar altimetry (Fricker and others, 2000a). The interferogram contains relative displacement information arising from tidal motion and ice flow. The difference in the predicted tidal heights at the ice front from the Circum-Antarctic Data Assimilation model (Padman and others, 2002) for these two passes is only ~2 cm and is uniform across the interferogram region (personal communication from L. Padman, 2001). Therefore, the observed phase change in Figure 6 is primarily due to ice flow. There are discontinuities in the phase across each of rifts A and B, and across the transverse (perpendicular-to-flow) fracture just beginning to form at the tip of rift A. The fringes across the ice between the rifts are orientated differently to that outside of the rifts. We suggest that this is because the loose tooth moves in a different manner to the rest of the ice shelf, as a result of the spreading of the fracture at its southwest corner. The loose tooth is apparently rotating clockwise in its embayment, and is hinged at the northeast or southeast corner. The fringes are further apart on the east side of rift A, indicating that it has experienced more relative motion than the ice on the west side, which is confirmed by the higher velocities there (Fig. 5). This is because the ice on the east side of rift A is undergoing additional motion due to the spreading rate of the transverse fracture. Fringes are also observed on the ice mélange within the rifts, suggesting that this ice is undergoing deformation as a result of the relative motion of the shelf ice on each side of the rift. This effect has also been observed within rifts on FIS by Rignot and MacAyeal (1998). These authors proposed that mélange may have sufficient mechanical structure that it plays a role in holding the two sides of the rift together, which can delay iceberg detachment.

There is a third longitudinal rift, beginning to form just east of centre in the loose tooth. The flowlines in Figure 3 indicate that this rift is associated with the suture formed at the western boundary of the Fisher Glacier flow-band. On the eastern side of the interferogram, discontinuities in the phase can be clearly seen across the crevasses (region C) discussed in section 3.1.

## 5. WHEN WILL THE AIS NEXT CALVE?

It is interesting to consider when the next major calving event will likely take place on the AIS. Surface velocity measurements made in situ in 1995 using global positioning system compared well with those made in 1968 using a theodolite and electronic distance meter (EDM) traverse along the middle of the AIS, suggesting that the ice shelf was in near-steady-state flow over this 27 year period in the mid-shelf region (Phillips, 1999). We therefore assume that the velocities at the ice-shelf front are also in steady state, and combine the location of the ice front in 2000 with the ice velocities shown in Figure 6 to estimate when the ice shelf will reach the last pre-calve (1963) position, taking into account the ice-shelf acceleration as it moves forward into Prydz Bay and thins. The AIS front still has not yet advanced half of the required distance (~70 km), and we conclude that the AIS will not experience a major calve until the mid-2020s or later. However, from the evidence presented here it appears that the portion of the ice shelf between the longitudinal rifts will calve around 10 years or more before that, perhaps around 2010–15.

The AIS is a stable system that is currently undergoing

changes that are part of its natural advance–calve–advance cycle. It is reasonable to suggest that this cycle might be repeatable with a period of 65–70 years. This is in contrast with the period given in Budd (1966) of 40 years.

## ACKNOWLEDGEMENTS

We would like to thank I. Joughin (JPL) and the RADARSAT Antarctic Mapping Program team for providing the RADARSAT imagery. RADARSAT data are © Canadian Space Agency 1997 and 2000. We also thank K. Watson and D. Sandwell (Scripps Institution of Oceanography (SIO)) for their help in generating the interferogram in Figure 6. ERS data were provided by the Alaska SAR Facility through NASA Research Announcement grant NRA-OES-99-10 and are © European Space Agency 1996. Thanks to B. Betts (SIO) for producing Figure 1. Thanks to T. Scambos and C. Hulbe for their role in initiating this short study, and to E. Rignot, K. Nicholls and an anonymous reviewer.

## REFERENCES

Budd, W. 1966. The dynamics of the Amery Ice Shelf. *J. Glaciol.*, **6**(45), 335–358.

Ferrigno, J. G. and W. G. Gould. 1987. Substantial changes in the coastline of Antarctica revealed by satellite imagery. *Polar Rec.*, **23**(146), 577–583.

Fricker, H. A., G. Hyland, R. Coleman and N. W. Young. 2000a. Digital elevation models for the Lambert Glacier–Amery Ice Shelf system, East Antarctica, from ERS-1 satellite radar altimetry. *J. Glaciol.*, **46**(155), 553–560.

Fricker, H. A., R. C. Warner and I. Allison. 2000b. Mass balance of the Lambert Glacier–Amery Ice Shelf system, East Antarctica: a comparison of computed balance fluxes and measured fluxes. *J. Glaciol.*, **46**(155), 561–570.

Fricker, H. A., S. Popov, I. Allison and N. Young. 2001. Distribution of marine ice under the Amery Ice Shelf, East Antarctica. *Geophys. Res. Lett.*, **28**(11), 2241–2244.

Fricker, H. A. *and 9 others*. In press. Redefinition of the grounding zone of the Lambert Glacier–Amery Ice Shelf system, East Antarctica. *J. Geophys. Res.*

Grosfeld, K., H. H. Hellmer, M. Jonas, H. Sandhäger, M. Schulte and D. G. Vaughan. 1998. Marine ice beneath Filchner Ice Shelf: evidence from a multi-disciplinary approach. *In* Jacobs, S. S. and R. F. Weiss, *eds. Ocean, ice and atmosphere: interactions at the Antarctic continental margin*. Washington, DC, American Geophysical Union, 321–341. (Antarctic Research Series 75.)

Hambrey, M. J. and J. A. Dowdeswell. 1994. Flow regime of the Lambert Glacier–Amery Ice Shelf system, Antarctica: structural evidence from Landsat imagery. *Ann. Glaciol.*, **20**, 401–406.

Jacobs, S. S., H. H. Hellmer, C. S. M. Doake, A. Jenkins and R. M. Frolich. 1992. Melting of ice shelves and the mass balance of Antarctica. *J. Glaciol.*, **38**(130), 375–387.

Jenkins, A. and A. Bombosch. 1995. Modeling the effects of frazil ice crystals on the dynamics and thermodynamics of ice shelf water plumes. *J. Geophys. Res.*, **100**(C4), 6967–6981.

Jezek, K. C. 1999. Glaciological properties of the Antarctic ice sheet from RADARSAT-1 synthetic aperture radar imagery. *Ann. Glaciol.*, **29**, 286–290.

Joughin, I. *and 7 others*. 1999. Tributaries of West Antarctic ice streams revealed by RADARSAT interferometry. *Science*, **286**(5438), 283–286.

Kipfstuhl, J., G. S. Dieckmann, H. Oerter, H. Hellmer and W. Graf. 1992. The origin of green icebergs in Antarctica. *J. Geophys. Res.*, **97**(C12), 20,319–20,324.

Lazzara, M. A., K. C. Jezek, T. A. Scambos, D. R. MacAyeal and C. J. van der Veen. 1999. On the recent calving of icebergs from the Ross Ice Shelf. *Polar Geogr.*, **23**(3), 201–212.

Lewis, E. L. and R. G. Perkin. 1986. Ice pumps and their rates. *J. Geophys. Res.*, **91**(C10), 11,756–11,762.

Padman, L., H. A. Fricker, R. Coleman, S. Howard and L. Erofeeva. 2002. A new tide model for the Antarctic ice shelves and seas. *Ann. Glaciol.*, **34** (see paper in this volume).

Phillips, H. A. 1999. Applications of ERS satellite radar altimetry in the Lambert Glacier–Amery Ice Shelf system, East Antarctica. (Ph.D. thesis, University of Tasmania.)

Rignot, E. and D. R. MacAyeal. 1998. Ice-shelf dynamics near the front of the Filchner–Ronne Ice Shelf, Antarctica, revealed by SAR interferometry. *J. Glaciol.*, **44**(147), 405–418.

Rignot, E. J., S. P. Gogineni, W. B. Krabill and S. Ekholm. 1997. North and north-east Greenland ice discharge from satellite radar interferometry. *Science*, **276**(5314), 934–937.

Robertson, B. 1992. Mass balance of the Amery Ice Shelf front. (Hon. thesis, University of Tasmania. Institute of Antarctic and Southern Ocean Studies.)

Swithinbank, C., P. McClain and P. Little. 1977. Drift tracks of Antarctic icebergs. *Polar Rec.*, **18**(116), 495–501.

Warren, S. G., C. S. Roesler, V. I. Morgan, R. E. Brandt, I. D. Goodwin and I. Allison. 1993. Green icebergs formed by freezing of organic-rich seawater to the base of Antarctic ice shelves. *J. Geophys. Res.*, **98**(C4), 6921–6928. (Correction: **98**(C10), 18,309.)

Young, N. and G. Hyland. 2002. Velocity and strain rates derived from InSAR analysis over the Amery Ice Shelf, East Antarctica. *Ann. Glaciol.*, **34** (see paper in this volume).

Young, N. W., D. Turner, G. Hyland and R. N. Williams. 1998. Near-coastal iceberg distributions in East Antarctica, 50–145° E. *Ann. Glaciol.*, **27**, 68–74.

Zwally, H. J., M. A. Beckley, A. C. Brenner and M. B. Giovinetto. 2002. Motion of major ice-shelf fronts in Antarctica from slant-range analysis of radar altimeter data, 1978–98. *Ann. Glaciol.*, **34** (see paper in this volume).